Earth and Planetary Science Letters 442 (2016) 72–79

Contents lists available at ScienceDirect

Earth and Planetary Science Letters

www.elsevier.com/locate/epsl

Crustal anisotropy and ductile flow beneath the eastern Tibetan Plateau and adjacent areas

Fansheng Kong [a], Jing Wu [b], Kelly H. Liu [a], Stephen S. Gao [a,*]

[a] Geology and Geophysics Program, Missouri University of Science and Technology, Rolla, MO 65409, USA
[b] State Key Laboratory of Lithospheric Evolution, Institute of Geology and Geophysics, Chinese Academy of Sciences, Beijing, China

ARTICLE INFO

Article history:
Received 4 December 2015
Received in revised form 23 February 2016
Accepted 1 March 2016
Available online 10 March 2016
Editor: A. Yin

Keywords:
seismic anisotropy
crustal flow
Tibetan Plateau
receiver functions

ABSTRACT

Crustal anisotropy beneath 71 broadband seismic stations situated at the eastern Tibetan Plateau and the Sichuan Basin is investigated based on the sinusoidal moveout of P-to-S conversions from the Moho and an intra-crustal discontinuity. Significant crustal anisotropy is pervasively detected beneath the study area with an average splitting time of 0.39 ± 0.18 s. The resulting fast orientations are mostly parallel to the major shear zones in the Songpan–Ganzi Terrane, and can be explained by fluid-filled fractures, favoring the model of rigid block motion with deformations concentrated on the block boundaries. In the vicinity of the Xianshuihe–Xiaojiang Fault Zone in the southern Songpan–Ganzi Terrane, our results, when combined with previously revealed high crustal Poisson's ratio in the area, support the existence of mid/lower crustal flow. The Longmenshan Fault Zone and adjacent areas are dominated by strike-orthogonal fast orientations, which are consistent with alignments of cracks associated with compressional stress between the Plateau and the Sichuan Basin. The observations suggest that crustal thickening is the main cause of the high topographic relief across the Longmenshan Fault Zone.

1. Introduction

The growth of the Tibetan Plateau, which has an average elevation of ~5000 m, is widely considered to be the result of progressive collision between the Indian and Eurasian plates, starting approximately 70 Ma (e.g., Yin and Harrison, 2000). N-S lithospheric shortening associated with the collision has resulted in eastward extrusion of the Plateau since about 15–20 Ma (Royden et al., 2008). Global Positioning System (GPS) velocity measurements (Gan et al., 2007) show eastward extrusion of central Tibet at a rate of about 15–20 mm/yr relative to the Sichuan Basin (Fig. 1). The bulk of the eastern Tibetan Plateau is the Songpan–Ganzi Terrane located between the Kunlun–Muztagh Suture to the north, the Jinsha River Suture to the south, and the Longmenshan Fault Zone to the east (Fig. 1). Blocks of the Songpan–Ganzi Terrane, including Aba, Litang, and Longmenshan, move relatively from each other along the sinistral Xianshuihe–Xiaojiang and dextral Longriba faults (Fig. 1), partially due to the blockage by the relatively rigid Sichuan Basin.

A recent study (Ji et al., 2015) suggests that the southeastward movement of the Litang Block resulted in the transformation of the E-W oriented, highly-foliated structures originally located at the Eastern Himalayan Syntaxis into NW-SE oriented tectonic fabrics. The present-day surface motion of the northern Songpan–Ganzi Terrane is characterized by a northward decreasing rate and a slight spatial variation of direction, indicating the presence of both compression and strike-slip shear deformations, which are also indicated by the pervasive thrust and strike-slip faults (Fig. 1). The eastern margin of the Tibetan Plateau, the Longmenshan Fault Zone, is characterized by a significant topographic relief relative to the plateau interior and the Sichuan Basin, with a low strike-orthogonal shortening rate of less than 3 mm/yr, but a high compressional stress rate (Gan et al., 2007). As discussed below, the fault zones contribute significantly to the observed crustal anisotropy, together with lower crustal flow and the aforementioned tectonic fabrics developed from foliated structures.

Mechanisms responsible for the expansion and uplifting of the eastern Tibetan Plateau remain enigmatic, in spite of numerous studies (e.g., Molnar and Tapponnier, 1975; England and Houseman, 1986; Royden et al., 1997; Gan et al., 2007; Bai et al., 2010; Liu et al., 2014a). Proposed geodynamic models applicable to eastern Tibet can be loosely divided into three groups. Those in the first group suggest a dominant role of a channeled ductile flow system in the mid/lower crust in the uplifting and lateral expansion of the Plateau (e.g., Bird, 1991; Royden et al., 1997;

* Corresponding author.
E-mail address: sgao@mst.edu (S.S. Gao).

http://dx.doi.org/10.1016/j.epsl.2016.03.003
0012-821X/

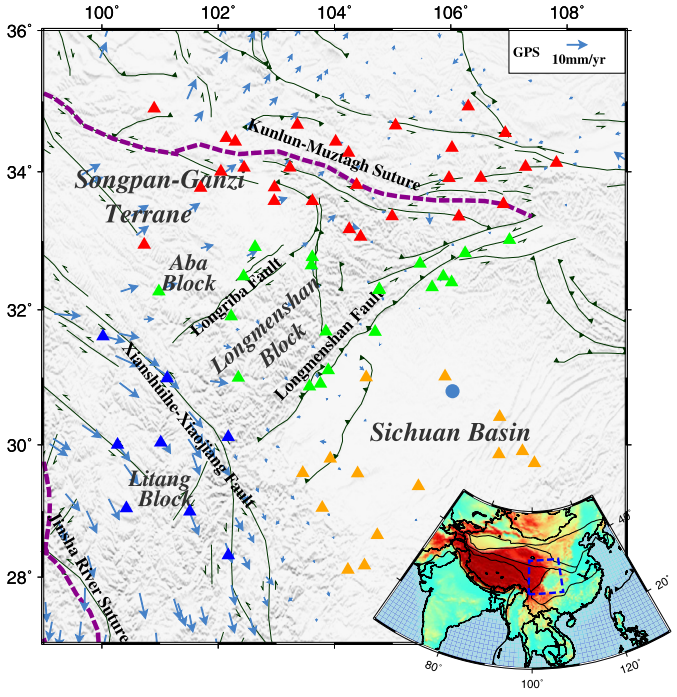

Fig. 1. A topographic relief map of the study area showing the suture zones (dashed purple lines), major faults (solid black lines), and seismic stations (triangles) used in the study. Different colors are assigned based on the sub-area that the station belongs to. Red: Kunlun–Muztagh Suture Zone; Green: Longmenshan Block and adjacent areas; Blue: Xianshuihe–Xiaojiang Fault Zone; Orange: Sichuan Basin. Light blue arrows show GPS velocities (Gan et al., 2007) relative to the solid blue circle in the Sichuan Basin. The Longriba Fault is digitized based on Ren et al. (2013), and the other faults are based on Styron et al. (2010). Dashed line in the inset map shows the location of the study area within Eurasia (For interpretation of the references to color in this figure legend, the reader is referred to the web version of this article.).

Clark and Royden, 2000; Burchfiel et al., 2008; Zhao et al., 2012). Those models are consistent with the general absence of upper-crustal thrust faults in the area. The second group of models advocate broadly distributed deformation of crustal shortening and thickening as a predominant mechanism (England and Houseman, 1986; Wang et al., 2008; Hubbard and Shaw, 2009). Those in the third group attribute the uplifting to successive developments of crustal thrust-wedges associated with the oblique subduction of the lithospheric mantle along major fault zones (Tapponnier et al., 1982, 2001; Replumaz and Tapponnier, 2003). One of the key constraints on the various models is a high-resolution quantification of crustal deformation, which can be characterized by seismic anisotropy measurements.

1.1. Formation mechanisms of crustal and mantle anisotropy

Numerous studies demonstrate that seismic azimuthal anisotropy, as quantified by the polarization orientation of the fast shear wave (ϕ) and the splitting delay time (δt) between the fast and slow shear waves, is a nearly ubiquitous property of the Earth's crust and mantle (Silver, 1996; Savage, 1999). It is generally believed that azimuthal anisotropy in the continental upper crust is mostly the result of shape preferred orientation of fluid-saturated vertical cracks (Crampin, 1981), which are sub-parallel to the maximum horizontal compression direction. The resulting δt is normally smaller than 0.2 s (Crampin, 1994), but can reach 0.5 s or greater for stations located in or close to a fault zone (e.g., Savage et al., 1990; Liu and Niu, 2012). Highly-deformed fabrics with a vertical foliation plane formed by compressional folding are also found to produce observable azimuthal anisotropy originating from anisotropic minerals in the crust such as mica and amphibole (Ji et al., 2015).

In the mid/lower crust, due to the closure of cracks, azimuthal anisotropy is mostly produced by the lattice preferred orientation (LPO) of anisotropic crystals, primarily amphibole (Tatham et al., 2008; Ko and Jung, 2015). A recent study of amphibole (Ko and Jung, 2015) suggests that channelized plastic flow in the mid/lower crust can result in azimuthal anisotropy. The relationship between the resulting ϕ and flow direction is dependent on the differential stress level and temperature (Fig. 2). Under the condition of high differential stress and high temperature, which is possible for the Tibetan Plateau due to significant crustal shortening and thickening (Yin and Harrison, 2000), type *II* and *III* fabrics, for which ϕ is sub-parallel to the flow direction, will dominate (Fig. 2).

Seismic anisotropy in the mantle is generally regarded as the consequence of LPO of anisotropic minerals, primarily olivine (Zhang and Karato, 1995). Mantle flow results in a fast orientation that is sub-parallel to the flow direction, and for areas experienced lithospheric shortening, the resulting ϕ is frequently observed in accordance with the strike of the mountain belt (e.g., McNamara et al., 1994; Silver, 1996; Bokelmann et al., 2013).

1.2. Previous seismic anisotropy investigations in the study area

Crustal and mantle azimuthal anisotropy beneath the eastern Tibetan Plateau has been investigated by a number of studies (e.g., Sol et al., 2007; Wang et al., 2008; Sun et al., 2012; Chen et al., 2013; Sun et al., 2015). Studies using the splitting of XKS phases (including SKS, SKKS, and PKS), which measure the integrated anisotropy of the crust and mantle, reveal an average splitting time of about 1.0 s. The fast orientations from XKS are mostly parallel to the strike of surface geological features (Fig. 3).

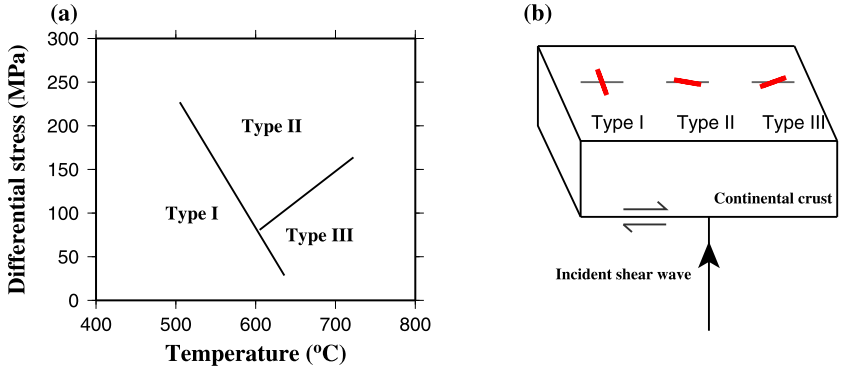

Fig. 2. (a) Types of amphibole fabrics as a function of differential stress and temperature. (b) Predicted seismic anisotropy formed by a horizontal flow system for a vertically propagating S-wave (Ko and Jung, 2015). On the top plane, the fast orientation is shown in red, and the flow direction is parallel to the gray bar. (For interpretation of the references to color in this figure legend, the reader is referred to the web version of this article.)

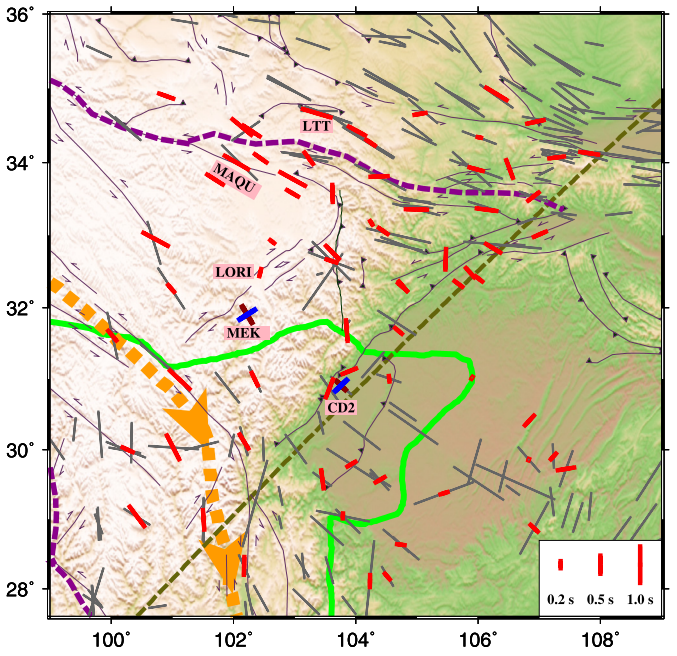

Fig. 3. Crustal anisotropy measurements (red) with orientation of the bars representing the ϕ, and the length proportional to the δt values. At stations MEK and CD2, the blue bar shows anisotropy of the upper layer, and the purple bar shows that of the lower layer. The gray bars are the station-averaged XKS splitting results obtained from http://splitting.gm.univ-montp2.fr/DB/public/searchdatabase.html. The area southwest of the green line is dominated by high Vp/Vs ratio ($\geq$1.78) from Wang et al. (2010). The orange dashed arrows show the location of proposed flow channel from Bai et al. (2010). The dashed line traversing the Longmenshan Fault Zone separates areas with large and small splitting times. (For interpretation of the references to color in this figure legend, the reader is referred to the web version of this article.)

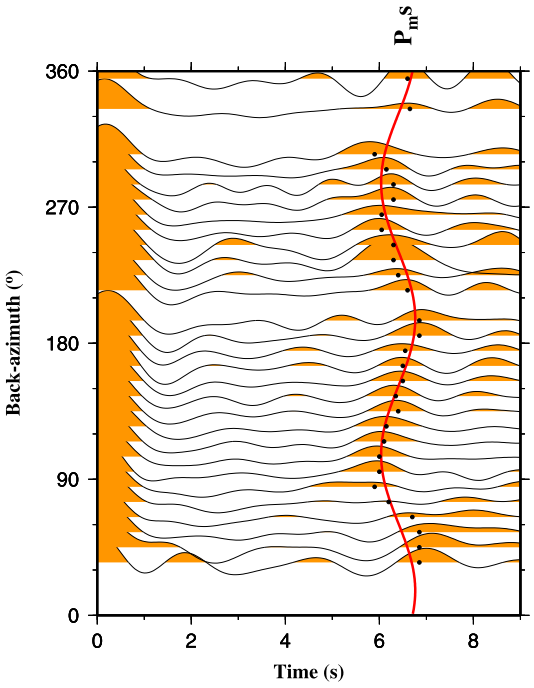

Fig. 4. Receiver functions recorded by station LTT. The black dots show the peak locations of the P_ms and the red line is the theoretical P_ms moveout calculated based on Equation (1) using the optimal pair of splitting parameters. (For interpretation of the references to color in this figure legend, the reader is referred to the web version of this article.)

Crustal anisotropy studies (e.g., Sun et al., 2012, 2015) suggest that the crust at some sites can produce large splitting times comparable to the global average of 1.0 s from XKS studies, suggesting a significant crustal contribution to the observed XKS splitting. A crustal anisotropy investigation (Sun et al., 2015) in the vicinity of the Longmenshan Fault Zone at 21 stations using the P-to-S converted phases from the Moho reports significant crustal anisotropy, with δt values ranging from 0.22 to 0.94 s. The observed anisotropy is attributed to the LPO of mica or amphibole deformed by lower crustal flow. The same formation mechanism of crustal anisotropy has been suggested beneath the Xianshuihe–Xiaojiang Fault Zone (e.g., Sun et al., 2012; Chen et al., 2013). In contrast, Ji et al. (2015) proposes that sub-vertical foliation planes, which lead to transverse isotropy with a horizontal axis of symmetry, are responsible for the observed crustal anisotropy beneath the study area.

In this study, crustal azimuthal anisotropy beneath the eastern Tibetan Plateau and adjacent areas is explored based on the sinusoidal moveout of the P-to-S converted phases from the Moho and (at a few stations) an intra-crustal discontinuity (Rumpker et al., 2014). The measurements have an average δt of 0.39 ± 0.18 s, and show dominantly fracture-parallel fast orientations.

2. Data and methods

2.1. Data

The broadband seismic data used in the study were recorded by 71 stations (Fig. 1), of which 53 were provided by the Data Management Centre of China National Seismic Network at Institute of Geophysics, China Earthquake Administration for the recording period of 2007–2011 (Zheng et al., 2010). Data from the other 18 stations were obtained from the Incorporated Research Institutions for Seismology (IRIS) Data Management Center (DMC) for the period of 2003–2014. All the teleseismic events with magnitude $\geq$4.0 and epicentral distance in the range of 30°–180° are band-pass filtered in the frequency band of 0.08–0.8 Hz, and those with visible first P-arrivals on the vertical component are converted to radial receiver functions (Ammon, 1991), which are visually inspected to select the ones with clear P-arrivals and without anomalously large arrivals in the P-wave coda. The two phases utilized in this study include P_ms, which is the P-to-S converted phase from the Moho for measuring the bulk crustal anisotropy, and P_is, which is the P-to-S converted phase from an intra-crustal interface for detecting upper crustal anisotropy at a few stations where P_is is clearly observed.

2.2. Detection of single layer of anisotropy

For a single layer of anisotropy with a horizontal axis of symmetry, the arrival times of the P-to-S converted phase (P_ms or P_is) vary systematically with the back-azimuth (BAZ) of the events (Liu and Niu, 2012; Rumpker et al., 2014), i.e.,

$$t = t_0 + \Delta t = t_0 - \frac{\delta t}{2}\cos[2(\alpha - \phi)], \quad (1)$$

where t_0 represents the arrival time in the isotropic case, Δt is the offset caused by crustal anisotropy along the raypath, δt is the delay time which reflects the strength of crustal anisotropy, ϕ is the fast orientation of crustal anisotropy measured clockwise from the north, and α is the BAZ of the events.

In this study, two pre-processing steps are applied to enhance the reliability of the measurements. First, in order to eliminate the moveout caused by epicentral distances, all the receiver function traces are adjusted to a uniform epicentral distance of 60°. Second, traces belonging to the same BAZ window of 10° wide are stacked together to enhance the signal-to-noise ratio. The splitting parameters, ϕ and δt, can be obtained by fitting the P_ms (or P_is) arrival times relative to the direct P-wave using Equation (1) based on a non-linear least-squares fitting procedure. An example can be found in Fig. 4.

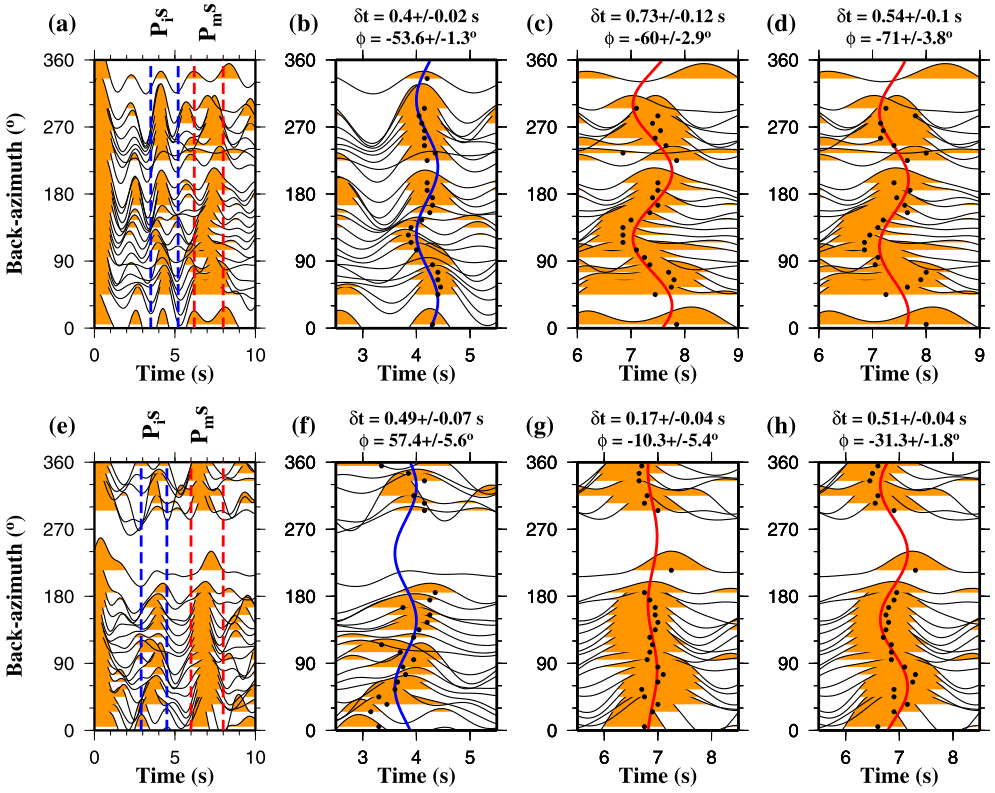

Fig. 5. Two-layer crustal anisotropy measurements using data recorded by stations MAQU (a)–(d) and MEK (e)–(h). (a) and (e) are the original receiver functions showing both the P_ms and P_is phases; (b) and (f) show the P_is arrivals and the fitting curve; (c) and (g) are the original P_ms arrivals, and (d) and (h) are P_ms arrivals after correcting for upper crustal anisotropy. (For interpretation of the colors in this figure, the reader is referred to the web version of this article.)

To quantify the uncertainties of the resulting crustal anisotropy measurements, we apply the bootstrap resampling procedure (Efron and Tibshirani, 1986; Press et al., 1992) to estimate the splitting parameters 10 times. The standard deviation (SD), σ, for the station is quantified by a unit-less value computed using

$$\sigma = \frac{\sigma_\phi}{90.0} + \frac{\sigma_{\delta t}}{1.0}, \tag{2}$$

where σ_ϕ and $\sigma_{\delta t}$ are the SD of ϕ and δt, respectively, estimated using the bootstrap procedure. Only results from stations with a $\sigma \leq 0.4$ are presented and discussed below.

2.3. Characterization of two layers of anisotropy

Two layers of crustal anisotropy are detected and characterized at 3 of the stations where a P_is phase is clearly identified in addition to the P_ms (Fig. 5), following the layer-stripping technique of Rumpker et al. (2014). For a given station with both P_ms and P_is arrivals, the P_is phases are used first to constrain the anisotropy in the layer above the interface ("upper crust"). The P_ms arrival times, which reflect the integrated effects of anisotropy in both the upper and lower crust, are then corrected using the resulting anisotropy parameters of the upper crust to remove the contributions of upper crustal anisotropy. The anisotropy of the lower layer can then be quantified by applying Equation (1) to the corrected P_ms traveltimes (Fig. 5).

In order to derive robust two layer crustal anisotropy measurements, some preconditions need to be satisfied: (1) the existence of an intra-crustal discontinuity, (2) clear and azimuthally varying P_is and P_ms arrivals, and (3) good back-azimuthal coverage of high-quality radial receiver functions. Only three of the stations, CD2, MAQU, and MEK, which are all located in the vicinity of known fault zones (Fig. 3), lead to reliable characterization of two-layer crustal anisotropy structure.

3. Results

Well-defined crustal anisotropy is measured at a total of 71 stations (Fig. 3). While the resulting ϕ measurements are dominantly parallel to the strike of major surface features, a sharp contrast of the δt values, which have an average value 0.39 ± 0.18 s, is observed between the Tibetan Plateau and the Sichuan Basin separated by the Longmenshan Fault Zone, with an mean value of 0.44 ± 0.18 s for the west, and 0.27 ± 0.13 s for the east (Fig. 6).

Comparison between our results and those by Chen et al. (2013) and Sun et al. (2015) are shown in Fig. 7. Chen et al. (2013) provided 33 crustal anisotropy measurements in our study area, and Sun et al. (2015) reported 21 measurements along the Longmenshan Fault Zone. While some differences exist at some stations (Fig. 7), the measurements from the 3 studies are generally consistent, in spite of the significantly larger spatial coverage that this study provides. As detailed in the Discussion section, the increased spatial coverage is essential for constraining anisotropy-forming mechanisms, as well as for providing valuable constraints for crustal deformation models.

Based on the major geologic features, we divide the study area into four regions, including the Kunlun–Muztagh Suture Zone, Xianshuihe–Xiaojiang Fault Zone, Longmenshan Block and adjacent areas, and the Sichuan Basin (Fig. 1).

3.1. Kunlun–Muztagh Suture Zone and Xianshuihe–Xiaojiang Fault Zone

Crustal anisotropy measurements from the 28 stations situated in the Kunlun–Muztagh Suture Zone (Fig. 1) result in an average δt of 0.47 ± 0.18 s. The ϕ measurements are dominantly ESE-WNW, consistent with the strike of the major faults. Fault-parallel fast orientations are also obtained at several stations in the same

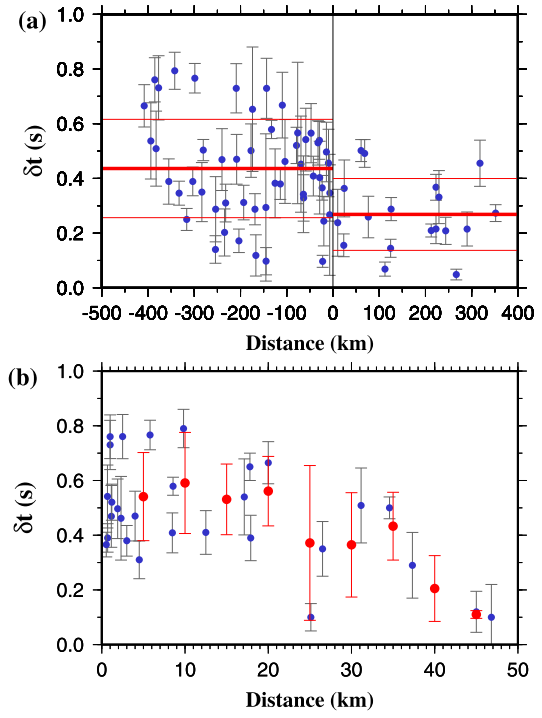

Fig. 6. (a) Splitting times from all stations with measurements plotted against the distance from the Longmenshan Fault Zone (the dashed line in Fig. 3). Thick horizontal bars represent mean values, and thin bars represent mean ± SD. (b) Splitting times from stations situated in the Kunlun–Muztagh Suture Zone plotted against the distance of stations to the nearest fault. Red dots show the moving averages in 10 km windows. (For interpretation of the references to color in this figure legend, the reader is referred to the web version of this article.)

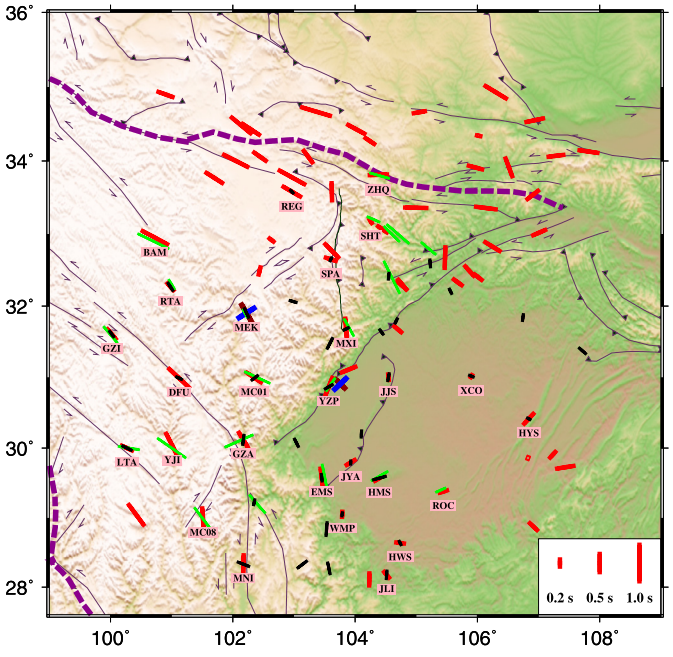

Fig. 7. Comparison between results from this study (red bars) and previous crustal anisotropy measurements from Chen et al. (2013) (black bars) and Sun et al. (2015) (green bars). (For interpretation of the references to color in this figure legend, the reader is referred to the web version of this article.)

area by a recent crustal anisotropy study (Wang et al., 2016). Station MAQU demonstrates the existence of two layers of anisotropy (Fig. 5), with comparable ϕ and δt values between the 2 layers. The similarity of anisotropy between the upper and lower crust

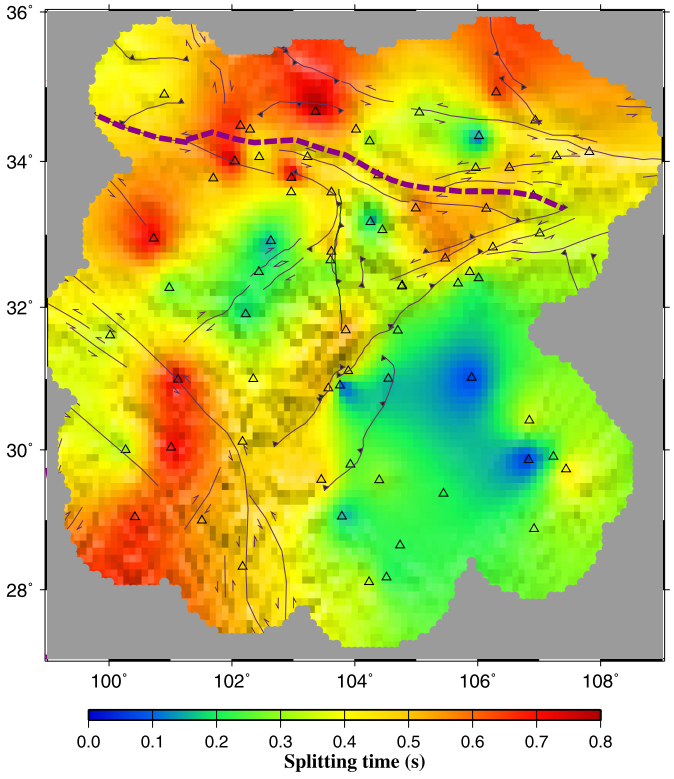

Fig. 8. Spatial distribution of the splitting times of crustal anisotropy measurements. To produce the data plotted here, a smooth surface was generated by fitting the observed values, with a spatial sampling interval of 0.1°. (For interpretation of the colors in this figure, the reader is referred to the web version of this article.)

may suggest that beneath the station, the entire crust deforms coherently.

Similarly, the Xianshuihe–Xiaojiang Fault Zone in the southern Songpan–Ganzi Terrane also exhibits large δt measurements (0.53 ± 0.16 s) and strike-parallel fast orientations. The Kunlun–Muztagh Suture Zone and Xianshuihe–Xiaojiang Fault Zone possess the largest δt values in the study area (Fig. 8).

3.2. Longmenshan Block and adjacent areas

The Longmenshan Block and adjacent areas between the Kunlun–Muztagh Suture Zone and the Xianshuihe–Xiaojiang Fault Zone are sampled by 20 stations. The ϕ measurements are dominantly NW-SE and the rest are mostly consistent with the NE-SW strike of faults (Fig. 3). The measurements from the 3 stations located at the Longriba Fault Zone are characterized by small δt with a mean value of 0.17 ± 0.03 s, and the fast orientations are either parallel or orthogonal to the strike of the faults. Measurements at station MEK (Fig. 5) suggest the presence of two anisotropic layers with orthogonal ϕ and comparable δt measurements. The ϕ of the lower layer is normal to the strike direction of the fault zone, and is strike-parallel for the upper layer.

The ϕ measurements from the 3 stations situated in the Longmenshan Fault Zone are parallel to the NE-SW strike of the faults, while the 8 stations situated in the adjacent areas of the faults are strike-orthogonal. The ϕ of the upper layer anisotropy beneath station CD2 is parallel to the strike of the Longmenshan Fault Zone, and that of the lower layer is orthogonal to it. Generally, the δt values along the Longmenshan Fault Zone are smaller than those obtained in the Kunlun–Muztagh Suture Zone and Xianshuihe–Xiaojiang Fault Zone, and the average δt is 0.35 ± 0.13 s (Fig. 8).

3.3. Sichuan Basin

The 15 stations located in the Sichuan Basin lead to a mean δt value of 0.25 ± 0.13 s, with smaller δt ($\leq$0.1 s) at stations in the interior of the basin. The ϕ measurements are mostly parallel to the surface fabric. The results are similar to those obtained by Sun et al. (2015) at 3 stations in the Sichuan Basin.

4. Discussion

4.1. Formation mechanisms of the observed crustal anisotropy and geodynamic implications

As discussed previously, a number of processes can lead to observable crustal anisotropy, including fluid-filled fracture zones, vertical foliation planes containing anisotropic minerals, and mid/lower crustal flow that aligns anisotropic minerals. For a given area, the relative importance of the processes is dependent on the tectonic setting and crustal properties such as thickness and Vp/Vs ratio (γ) which is uniquely related to the better-known Poisson's ratio (σ) by $\sigma = 0.5[1 - 1/(\gamma^2 - 1)]$. In this section, we speculate on the formation mechanisms for each of the areas on the basis of existing surface geology and crustal property observations, as well as their relationship with the observed crustal anisotropy parameters.

4.1.1. Kunlun–Muztagh Suture Zone

Significant crustal anisotropy is observed throughout the Kunlun–Muztagh Suture Zone, with the ϕ measurements being dominantly parallel to the major faults in the suture zone. Previous receiver function studies of the crust report Vp/Vs values of about 1.73 which are lower than the global average of 1.76 for continental crust (e.g., Wang et al., 2010; Sun et al., 2015), suggesting the absence of large-scale crustal partial melting, which would lead to much higher Vp/Vs values (e.g., Reed et al., 2014). Vertically coherent crustal-mantle deformation and a possible absence of lower crustal flow beneath this area are also suggested by a recent study of Wang et al. (2016), who observed low crustal Vp/Vs ratio and strong fault-parallel crustal and mantle anisotropy.

To explore the relationship between crustal anisotropy measurements and the faults, we plot the observed splitting times against the distance of the stations from the nearest fault. As shown in Fig. 6b, for stations within 20 km from the nearest fault, the splitting times are the largest (about 0.6 s) and are not varying with the distance, implying the existence of a broad shear zone at depth. For stations that are more than 20 km away from the fault, there seems to be a gradual decrease in the splitting times with increasing distance. This relationship, together with the fact that the fast orientations are mostly parallel to the strike of the faults in the suture zone, suggests that crustal anisotropy in this area is mostly related to fractures associated with the suture zone.

4.1.2. Xianshuihe–Xiaojiang Fault Zone

Similar to the Kunlun–Muztagh Suture Zone, the Xianshuihe–Xiaojiang Fault Zone is characterized by fault-strike-parallel fast orientations (Fig. 3) and large splitting times (Fig. 8). However, unlike the former, an inverse relationship between the splitting times and the distance to the nearest fault is not robustly observed. This could indicate that unlike those in the suture zone, fractures in the Xianshuihe–Xiaojiang Fault Zone have a limited lateral extent and thus contribute insignificantly to the observed crustal anisotropy.

Another difference between the two areas is that while the former has lower than normal crustal Vp/Vs values, the latter is dominated by high Vp/Vs values ($\geq$1.78; Fig. 3) and thus may indicate the existence of crustal partial melting (e.g., Wang et al., 2010; Sun et al., 2015). This is independently evidenced by the high electrical conductivity observed beneath this area (Bai et al., 2010), and may reflect plastic flow in the mid/lower crust toward the southeast (Clark and Royden, 2000; Bai et al., 2010). The consistency between the fast orientations and the predicted flow direction suggests that the dominant LPO of amphibole in the area is Type *II* or Type *III* (Fig. 2), which results in a flow-parallel fast orientation for a vertically propagating S-wave (Ko and Jung, 2015).

Besides faults in the upper crust and plastic flow in the mid/lower crust, another potential contributor to the observed anisotropy in this area is shear-related mineral lineation. A recent study (Ji et al., 2015) reveals sub-vertically aligned foliation planes with nearly horizontal lineations in the southeastern Tibetan Plateau, which are being rotated through strike-slip shear around the Himalayan Syntaxis. The NW-SE oriented foliation planes contain mica- and amphibole-bearing metamorphic rocks, leading to significant transverse isotropy with a horizontal axis of symmetry. The resulting fast orientation for a vertically propagating S-wave is in the foliation plane and parallel to the lineation direction.

4.1.3. Longmenshan Block and adjacent areas

Relative to other areas of the eastern Tibetan Plateau, this area has the weakest crustal anisotropy (Fig. 8), in spite of the fact that it is experiencing a high rate of NW-SE directed compressional stress (Gan et al., 2007). The consistency between the fast orientations and the direction of the maximum horizontal compression suggests that NW-SE oriented extensional cracks in the upper crust are mostly responsible for the observed anisotropy. Such a mechanism is commonly involved to explain crustal anisotropy in areas dominated by compressional tectonics (Crampin, 1981, 1994). Station LORI in the Longriba Fault Zone and a few stations along the Longmenshan Fault show fault-parallel fast orientations and small splitting times, probably related to fluid-filled fractures in the fault zones. This mechanism can also explain the NE-SW directed fast orientation of the upper layer at stations MEK and CD2. Alternatively, the 90° difference between upper and lower crustal anisotropy can be caused by a previously revealed 90° flip as a result of pore pressure exceeding the maximum horizontal compressional stress (Crampin et al., 2003). This mechanism implies a high pore pressure in the upper crust at the stations with two-layer anisotropy.

Crustal anisotropy studies (Shi et al., 2009; Gao et al., 2014) using shear waves from local earthquakes show mostly fault-parallel fast orientations at stations located in the north-most 100 km of the Longmenshan Fault zone, while our results are mostly fault-orthogonal in the same area. This apparent discrepancy could be caused by the fact that the former studies measure the anisotropy of the seismogenic upper crust, while our results are integrated over the whole crust. The fact that the crustal anisotropy has a fault-orthogonal fast orientation suggests that the lower crust has a NW-SE oriented anisotropy with a much larger splitting time than the upper crust.

The small splitting times may suggest the absence of strong mid/lower crustal flow beneath this area. The blockage of the Sichuan Basin might be responsible for the absence, although the study alone cannot rule out the existence of partial melting in the mid/lower crust. However, the normal Vp/Vs values observed in most of the area (Wang et al., 2010) place doubts on the existence of significant crustal partial melting (e.g., Clark and Royden, 2000; Zhao et al., 2012), but support a crustal thickening model for the dramatic topographic relief and recent large earthquakes in the Longmenshan Fault Zone (e.g., Hubbard and Shaw, 2009; Wang et al., 2012).

4.1.4. Sichuan Basin

The crust beneath the Sichuan Basin is weakly anisotropic, as indicated by the smallest average splitting time in the entire study area (Fig. 8), an observation that is consistent with the previously suggested strong lithosphere beneath the basin (Huang et al., 2015). Most of the fast orientations in the basin are NE-SW which might reflect the strike of crustal fabrics formed by ancient tectonic events. The several stations near the SW edge of the basin show edge-parallel fast orientations and could indicate the existence and reflect the effects of major boundary faults.

4.2. Implications on mantle deformation

For all of the study area, with possible exception of the Sichuan Basin, the fast orientation of crustal anisotropy is dominantly consistent with that of the XKS measurements, which represent the integrated anisotropy of both the crust and mantle. As shown in Fig. 3, in which the P_ms and XKS splitting parameters are plotted using the same scale, although crustal anisotropy is a significant contributor to the observed XKS anisotropy for most areas, the fact that XKS splitting times are constantly greater than P_ms splitting times suggests that the mantle is also anisotropic.

The observed mantle anisotropy can be explained by two models. The first is the coherent lithospheric deformation model for which both the crustal and mantle portions of the lithosphere deform as an entity (Silver, 1996; Wang et al., 2008). For the mantle portion, this model attributes the suture- or fault-parallel mantle anisotropy to strike-orthogonal compression, which orients the olivine a-axis to the strike direction (Silver, 1996). Because the dominant faults are strike-slip, and strike-slip faults are inefficient in re-orienting mantle anisotropic minerals (e.g., Liu et al., 2014b for the San Andreas Fault), it is difficult to attribute the observed mantle anisotropy to coherent lithospheric deformation.

The second and our preferred model is that mantle anisotropy is caused by simple shear in the upper-most asthenosphere due to its differential movement with the lithosphere. Such a mechanism is widely used to explain XKS anisotropy (e.g., Refayee et al., 2014 for central North America, and Lemnifi et al., 2015 for North Africa). The differential movement can be induced by lithospheric movement along the strike-slip faults over a stationary asthenosphere, or by a faster- or slower-moving asthenospheric flow in the direction of the major fault zones.

5. Conclusions

P-to-S conversion from the Moho and an intra-crustal discontinuity reveals strong and spatially varying crustal anisotropy beneath the eastern Tibetan Plateau and Sichuan Basin, with unprecedented spatial resolution. For most of the study area, the resulting fast orientations are dominantly parallel to the strike of major strike-slip faults, and the largest splitting times are found in major shear zones. Beneath the vicinity of the Xianshuihe–Xiaojiang Fault Zone, our results support the existence of mid/lower crustal flow. The pervasive strike-orthogonal fast orientations in the vicinity of the Longmenshan Fault Zone suggest a significant contribution of fault-normal compressional stress to the large topographic relief across the fault.

Acknowledgements

We thank the Data Management Centre of China National Seismic Network at Institute of Geophysics, China Earthquake Administration (SEISDMC, http://dx.doi.org/10.7914/SN/CB) and the IRIS DMC for providing the seismic data. Youqiang Yu helped with the format conversion of the data sets. The study was partially supported by the United States National Science Foundation under grant EAR-0911346 to K.L. and S.G., and by the Natural Science Foundation of China under awards 41374064 and 41574055 to J.W.

References

Ammon, C.J., 1991. The isolation of receiver effects from teleseismic P waveforms. Bull. Seismol. Soc. Am. 81, 2504–2510.

Bai, D., Unsworth, M.J., Meju, M.A., Ma, X., Teng, J., Kong, X., Sun, Y., Sun, J., Wang, L., Jiang, C., Zhao, C., Xiao, P., Liu, M., 2010. Crustal deformation of the eastern Tibetan plateau revealed by magnetotelluric imaging. Nat. Geosci. 3, 358–362. http://dx.doi.org/10.1038/NGEO830.

Bird, P., 1991. Lateral extrusion of lower crust from under high topography in the isostatic limit. J. Geophys. Res. 96, 10275–10286. http://dx.doi.org/10.1029/91JB00370.

Bokelmann, G., Qorbani, E., Bianchi, I., 2013. Seismic anisotropy and large-scale deformation of the Eastern Alps. Earth Planet. Sci. Lett. 383, 1–6. http://dx.doi.org/10.1016/j.epsl.2013.09.019.

Burchfiel, B.C., Royden, L.H., van der Hilst, R.D., Hager, B.H., Chen, Z., King, R.W., Li, C., Lu, J., Yao, H., Kirby, E., 2008. A geological and geophysical context for the Wenchuan earthquake of 12 May 2008, Sichuan, People's Republic of China. GSA Today 18 (7). http://dx.doi.org/10.1130/GSATG18A.1.

Chen, Y., Zhang, Z., Sun, C., Badal, J., 2013. Crustal anisotropy from Moho converted Ps wave splitting analysis and geodynamic implications beneath the eastern margin of Tibet and surrounding regions. Gondwana Res. 24, 946–957. http://dx.doi.org/10.1016/j.gr.2012.04.003.

Clark, M.K., Royden, L.H., 2000. Topographic ooze: building the eastern margin of Tibet by lower crustal flow. Geology 28, 703–706. http://dx.doi.org/10.1130/0091-7613(2000)28<703:TOBTEM>2.0.CO;2.

Crampin, S., 1981. A review of wave motion in anisotropic and cracked elastic-media. Wave Motion 3, 343–391. http://dx.doi.org/10.1016/0165-2125(81)90026-3.

Crampin, S., 1994. The fracture criticality of crustal rocks. Geophys. J. Int. 118, 428–438. http://dx.doi.org/10.1111/j.1365-246X.1994.tb03974.x.

Crampin, S., Chastin, S., Gao, Y., 2003. Shear-wave splitting in a critical crust: III preliminary report of multi-variable measurements in active tectonics. J. Appl. Geophys. 54, 265–277. http://dx.doi.org/10.1016/j.jappgeo.2003.01.001.

Efron, B., Tibshirani, R., 1986. Bootstrap methods for standard errors, confidence intervals, and other measures of statistical accuracy. Stat. Sci. 1, 54–75. http://dx.doi.org/10.1214/ss/1177013815.

England, P., Houseman, G., 1986. Finite strain calculations of continental deformation: 2. Comparison with the India–Asia collision zone. J. Geophys. Res. 91, 3664–3676. http://dx.doi.org/10.1029/JB091iB03p03664.

Gan, W., Zhang, P., Shen, Z., Niu, Z., Wang, M., Wan, Y., Zhou, D., Cheng, J., 2007. Present-day crustal motion within the Tibetan Plateau inferred from GPS measurements. J. Geophys. Res. 112, B08416. http://dx.doi.org/10.1029/2005JB004120.

Gao, Y., Wang, Q., Zhao, B., Shi, Y., 2014. A rupture blank zone in middle south part of Longmenshan Faults: effect after Lushan Ms7.0 earthquake of 20 April 2013 in Sichuan, China. Sci. China Earth Sci. 57, 2036–2044. http://dx.doi.org/10.1007/s11430-014-4827-2.

Huang, Z., Wang, P., Xu, M., Wang, L., Ding, Z., Wu, Y., Xu, M., Mi, N., Yu, D., Li, H., 2015. Mantle structure and dynamics beneath SE Tibet revealed by new seismic images. Earth Planet. Sci. Lett. 411, 100–111. http://dx.doi.org/10.1016/j.epsl.2014.11.040.

Hubbard, J., Shaw, J.H., 2009. Uplift of the Longmen Shan and Tibetan plateau, and the 2008 Wenchuan (M = 7.9) earthquake. Nature 458, 194–197. http://dx.doi.org/10.1038/nature07837.

Ji, S., Shao, T., Michibayashi, K., Oya, S., Satsukawa, T., Wang, Q., Zhao, W., Salisbury, M.H., 2015. Magnitude and symmetry of seismic anisotropy in mica- and amphibole-bearing metamorphic rocks and implications for tectonic interpretation of seismic data from the southeast Tibetan Plateau. J. Geophys. Res. 120, 6404–6430. http://dx.doi.org/10.1002/2015JB012209.

Ko, B., Jung, H., 2015. Crystal preferred orientation of an amphibole experimentally deformed by simple shear. Nat. Commun. 6, 6586. http://dx.doi.org/10.1038/ncomms7586.

Lemnifi, A.A., Liu, K.H., Gao, S.S., Reed, C.A., Elsheikh, A.A., Yu, Y., Elmelade, A.A., 2015. Azimuthal anisotropy beneath north central Africa from shear wave splitting analyses. Geochem. Geophys. Geosyst. 16, 1105–1114. http://dx.doi.org/10.1002/2014GC005706.

Liu, H., Niu, F., 2012. Estimating crustal seismic anisotropy with a joint analysis of radial and transverse receiver function data. Geophys. J. Int. 188, 144–164. http://dx.doi.org/10.1111/j.1365-246X.2011.05249.x.

Liu, Q.Y., van der Hilst, R.D., Li, Y., Yao, H.J., Chen, J.H., Guo, B., Qi, S.H., Wang, J., Huang, H., Li, S.C., 2014a. Eastward expansion of the Tibetan Plateau by crustal flow and strain partitioning across faults. Nat. Geosci. 7, 361–365. http://dx.doi.org/10.1038/ngeo2130.

Liu, K.H., Elsheikh, A., Lemnifi, A., Purevsuren, U., Ray, M., Refayee, H., Yang, B.B., Yu, Y., Gao, S.S., 2014b. A uniform database of teleseismic shear wave splitting measurements for the western and central United States. Geochem. Geophys. Geosyst. 15, 2075–2085. http://dx.doi.org/10.1002/2014GC005267.

McNamara, D., Owens, T.J., Silver, P.G., Wu, F.T., 1994. Shear wave anisotropy beneath the Tibetan Plateau. J. Geophys. Res. 99, 13655–13665. http://dx.doi.org/10.1029/93JB03406.

Molnar, P., Tapponnier, P., 1975. Cenozoic tectonics of Asia: effects of a continental collision. Science 189, 419–426. http://dx.doi.org/10.1126/science.189.4201.419.

Press, W.H., Teukolsky, S.A., Vetterling, W.T., Flannery, B.P., 1992. Numerical Recipes in FORTRAN, second ed. Cambridge Univ. Press.

Reed, C.A., Almadani, S., Gao, S.S., Elsheikh, A.A., Cherie, S., Abdelsalam, M.G., Thurmond, A.K., Liu, K.H., 2014. Receiver function constraints on crustal seismic velocities and partial melting beneath the Red Sea rift and adjacent regions, Afar Depression. J. Geophys. Res. 119, 2138–2152. http://dx.doi.org/10.1002/2013JB010719.

Refayee, H.A., Yang, B.B., Liu, K.H., Gao, S.S., 2014. Mantle flow and lithosphere–asthenosphere coupling beneath the southwestern edge of the North American craton: constraints from shear-wave splitting measurements. Earth Planet. Sci. Lett. 402, 209–220. http://dx.doi.org/10.1016/j.epsl.2013.01.031.

Ren, J., Xu, X., Yeats, R.S., Zhang, S., 2013. Latest Quaternary paleoseismology and slip rates of the Longriba fault zone, eastern Tibet: implications for fault behavior and strain partitioning. Tectonics 32, 216–238. http://dx.doi.org/10.1002/tect.20029.

Replumaz, A., Tapponnier, P., 2003. Reconstruction of the deformed collision zone between India and Asia by backward motion of lithospheric blocks. J. Geophys. Res. 108, 2285. http://dx.doi.org/10.1029/2001JB000661.

Royden, L.H., Burchfiel, B.C., King, R.W., Wang, E., Chen, Z., Shen, F., Liu, Y., 1997. Surface deformation and lower crustal flow in eastern Tibet. Science 276, 788–790. http://dx.doi.org/10.1126/science.276.5313.788.

Royden, L.H., Burchfiel, B.C., van der Hilst, R.D., 2008. The geological evolution of the Tibetan Plateau. Science 321, 1054–1058. http://dx.doi.org/10.1126/science.1155371.

Rumpker, G., Kaviani, A., Latifi, K., 2014. Ps-splitting analysis for multilayered anisotropic media by azimuthal stacking and layer stripping. Geophys. J. Int. 199, 146–163. http://dx.doi.org/10.1093/gji/ggu154.

Savage, M.K., Peppin, W.A., Vetter, U.R., 1990. Shear wave anisotropy and stress direction in and near Long Valley Caldera, California, 1979–1988. J. Geophys. Res. 95, 11165–11177. http://dx.doi.org/10.1029/JB095iB07p11165.

Savage, M.K., 1999. Seismic anisotropy and mantle deformation: what have we learned from shear wave splitting? Rev. Geophys. 37, 65–106. http://dx.doi.org/10.1029/98RG02075.

Shi, Y., Gao, Y., Zhao, C., Yao, Z., Tai, L., 2009. A study of seismic anisotropy of Wenchuan earthquake sequence. Chin. J. Geophys. 52, 138–147. http://dx.doi.org/10.1002/cjg2.1335.

Silver, P.G., 1996. Seismic anisotropy beneath the continents: probing the depths of geology. Annu. Rev. Earth Planet. Sci. 24, 385–432. http://dx.doi.org/10.1146/annurev.earth.24.1.385.

Sol, S., Meltzer, A., Burgmann, R., van der Hilst, R.D., King, R., Chen, Z., Koons, P.O., Lev, E., Liu, Y.P., Zeitler, P.K., Zhang, X., Zhang, J., Zurek, B., 2007. Geodynamics of the southeastern Tibetan Plateau from seismic anisotropy and geodesy. Geology 35, 563–566. http://dx.doi.org/10.1130/G23408A.1.

Styron, R., Taylor, M., Okoronkwo, K., 2010. Database of active structures from the Indo-Asian collision. Eos Trans. AGU 91, 181–182. http://dx.doi.org/10.1029/2010EO200001.

Sun, Y., Niu, F., Liu, H., Chen, Y., Liu, J., 2012. Crustal structure and deformation of the SE Tibetan plateau revealed by receiver function data. Earth Planet. Sci. Lett. 349, 186–197. http://dx.doi.org/10.1016/j.epsl.2012.07.007.

Sun, Y., Liu, J., Zhou, K., Chen, B., Guo, R., 2015. Crustal structure and deformation under the Longmenshan and its surroundings revealed by receiver function data. Phys. Earth Planet. Inter. 244, 11–22. http://dx.doi.org/10.1016/j.pepi.2015.04.005.

Tapponnier, P., Peltzer, G., Le Dain, A.Y., Armijo, R., Cobbold, P., 1982. Propagating extrusion tectonics in Asia: new insights from simple experiments with plasticine. Geology 10, 611–616. http://dx.doi.org/10.1130/0091-7613(1982)10<611:PETIAN>2.0.CO;2.

Tapponnier, P., Xu, Z., Roger, F., Meyer, B., Arnaud, N., Wittlinger, G., Yang, J., 2001. Oblique stepwise rise and growth of the Tibet Plateau. Science 294, 1671–1677. http://dx.doi.org/10.1126/science.105978.

Tatham, D.J., Lloyd, G.E., Butler, R.W.H., Casey, M., 2008. Amphibole and lower crustal seismic properties. Earth Planet. Sci. Lett. 267, 118–128. http://dx.doi.org/10.1016/j.epsl.2007.11.042.

Wang, C., Flesch, L.M., Silver, P.G., Chang, L., Chan, W.W., 2008. Evidence for mechanically coupled lithosphere in central Asia and resulting implications. Geology 36, 363–366. http://dx.doi.org/10.1130/G24450A.1.

Wang, E., Kirby, E., Furlong, K.P., van Soest, M., Xu, G., Shi, X., Kamp, P.J.J., Hodges, K.V., 2012. Two-phase growth of high topography in eastern Tibet during the Cenozoic. Nat. Geosci. 5, 640–645. http://dx.doi.org/10.1038/ngeo1538.

Wang, Q., Niu, F., Gao, Y., Chen, Y., 2016. Crustal structure and deformation beneath the NE margin of the Tibetan plateau constrained by teleseismic receiver function data. Geophys. J. Int. 204, 167–179. http://dx.doi.org/10.1093/gji/ggv420.

Wang, C., Zhu, L., Lou, H., Huang, B., Yao, Z., Luo, X., 2010. Crustal thicknesses and Poisson's ratios in the eastern Tibetan Plateau and their tectonic implications. J. Geophys. Res. 115, B11301. http://dx.doi.org/10.1029/2010JB007527.

Yin, A., Harrison, T.M., 2000. Geologic evolution of the Himalayan–Tibetan orogen. Annu. Rev. Earth Planet. Sci. 28, 211–280. http://dx.doi.org/10.1146/annurev.earth.28.1.211.

Zhang, S., Karato, S.I., 1995. Lattice preferred orientation of olivine aggregates deformed in simple shear. Nature 375, 774–777. http://dx.doi.org/10.1038/375774a0.

Zhao, G., Unsworth, M.J., Zhan, Y., Wang, L., Chen, X., Jones, A.G., Tang, J., Xiao, Q., Wang, J., Cai, J., Li, T., Wang, Y., Zhang, J., 2012. Crustal structure and rheology of the Longmenshan and Wenchuan Mw 7.9 earthquake epicentral area from magnetotelluric data. Geology 40, 1139–1142. http://dx.doi.org/10.1130/G33703.1.

Zheng, X., Yao, Z., Liang, J., Zheng, J., 2010. The role played and opportunities provided by IGP DMC of China National Seismic Network in Wenchuan earthquake disaster relief and researches. Bull. Seismol. Soc. Am. 100, 2866–2872. http://dx.doi.org/10.1785/0120090257.